SeaWiFS long-term solar diffuser reflectance and sensor noise analyses

Robert E. Eplee, Jr., Frederick S. Patt, Robert A. Barnes, and Charles R. McClain

The NASA Ocean Biology Processing Group's Calibration and Validation (Cal/Val) team has undertaken an analysis of the mission-long Sea-Viewing Wide Field-of-View Sensor (SeaWiFS) solar calibration time series to assess the long-term degradation of the solar diffuser reflectance over 9 years on orbit. The SeaWiFS diffuser is an aluminum plate coated with YB71 paint. The bidirectional reflectance distribution function of the diffuser was not fully characterized before launch, so the Cal/Val team has implemented a regression of the solar incidence angles and the drift in the node of the satellite's orbit against the diffuser time series to correct for solar incidence angle effects. An exponential function with a time constant of 200 days yields the best fit to the diffuser time series. The decrease in diffuser reflectance over the mission is wavelength dependent, ranging from 9% in the blue (412 nm) to 5% in the red and near infrared (670–865 nm). The Cal/Val team has developed a methodology for computing the signal-to-noise ratio (SNR) for SeaWiFS on orbit from the diffuser time series corrected for both the varying solar incidence angles and the diffuser reflectance degradation. A sensor noise model is used to compare on-orbit SNRs computed for radiances reflected from the diffuser with prelaunch SNRs measured at typical radiances specified for the instrument. To within the uncertainties in the measurements, the SNRs for SeaWiFS have not changed over the mission. The on-orbit performance of the SeaWiFS solar diffuser should offer insight into the long-term on-orbit performance of solar diffusers on other instruments, such as the Moderate-Resolution Imaging Spectrometer [currently flying on the Earth Observing System (EOS) Terra and Aqua satellites], the Visible and Infrared Radiometer Suite [scheduled to fly on the NASA National Polar-orbiting Operational Environmental Satellite System (NPOESS) and NPOESS Preparatory Project (NPP) satellites] and the Advanced Baseline Imager [scheduled to fly on the National Oceanic and Atmospheric Administration Geostationary Environmental Operational Satellite Series R (GOES-R) satellites]. © 2007 Optical Society of America

OCIS codes: 280.0280, 120.0280, 230.1980, 010.0010, 120.5630, 120.0120.

1. Introduction

The Sea-Viewing Wide Field-of-View Sensor (SeaWiFS) is an eight-band visible and near-infrared scanning radiometer designed to have high radiometric sensitivity over oceans without saturating over bright clouds. The bands are provided in Table 1. The goal of the NASA Ocean Biology Processing Group's Calibration and Validation (Cal/Val) team is to produce a long-term ocean color data set with 5% absolute and 1% relative accuracies on the water-leaving radiances and 35% accuracy on chlorophyll a concentrations in open-ocean regions.[1] To meet this goal, the Cal/Val team has implemented an on-orbit calibration strategy that uses monthly lunar calibrations to monitor the radiometric stability of the instrument over its mission lifetime and that uses daily solar calibrations to look for short-period, step-function changes in the instrument response.[2,3] The Cal/Val team has undertaken an analysis of the mission-long solar calibration time series to assess the long-term degradation in the solar diffuser reflectance over 9 years on orbit. SeaWiFS presents advantages for this analysis since the diffuser is not the primary monitor of the instrument's radiometric stability. This analysis has allowed the Cal/Val team to use the sunlight reflected from the diffuser to compute the signal-to-noise ratios (SNRs) of the instrument on orbit and to monitor changes in the SNRs over time.

R. E. Eplee, Jr. (eplee@seawifs.gsfc.nasa.gov), F. S. Patt, and R. A. Barnes are with Science Applications International Corporation, 4600 Powder Mill Road, Suite 400, Beltsville, Maryland 20705, USA. C. R. McClain is with the Ocean Biology Processing Group, NASA Goddard Space Flight Center, Mail Code 614.8, Greenbelt, Maryland 20771, USA.

Received 24 May 2006; revised 1 September 2006; accepted 6 October 2006; posted 17 October 2006 (Doc. ID 71360); published 25 January 2007.

0003-6935/07/050762-12$15.00/0

© 2007 Optical Society of America

Table 1. SeaWiFS Bands[a]

Band	1	2	3	4	5	6	7	8
Wavelength	412	443	490	510	555	670	765	865
Bandwidth	20	20	20	20	20	20	40	40

[a]The nominal center wavelengths and bandwidths are in nanometers.

2. Lunar Calibration Background

The solar diffuser data studied in this analysis have been calibrated with the operational SeaWiFS calibration table, so the data have been corrected for changes in the radiometric response of the instrument over time. The derivation of the lunar-based radiometric corrections is reviewed briefly here.

The Cal/Val team has analyzed the mission-long SeaWiFS lunar calibration time series, encompassing 104 monthly lunar observations spanning some 3200 days from November 1997 through July 2006. During a lunar calibration, the spacecraft is pitched across the Moon so that SeaWiFS views the Moon near nadir through the same optical path as it views the Earth. The changes in radiometric response of the instrument are monitored through the same optical path as the Earth data are collected. The scan angles of the lunar observations are distributed over the range of $-15°$ to $+18°$, and the same scan modulation corrections are applied to both the lunar and the Earth data. Consequently, the changes in the radiometric response of the instrument are independent of the angles of incidence of the lunar data.[4] The individual lunar observations have been normalized to a common viewing geometry for the radiometric stability analysis. Corrections computed from the time and geometry of the observations include Sun–Moon and instrument–Moon distances, oversampling of the lunar image (computed from the measured size of the lunar images in the along-track direction), and variations in the phase and libration angles of the Moon during the observations.[5,6] The Cal/Val team has fit the corrected lunar calibration time series by two simultaneous decaying exponential functions of time, with time constants of 200 and 2500 days,[7] as shown in Fig. 1. The inverses of these fits constitute the radiometric corrections that are incorporated into the SeaWiFS calibration table. Since the Cal/Val team uses lunar observations to derive the radiometric calibration of SeaWiFS over time, the Moon acts as a de facto solar diffuser stability monitor for SeaWiFS, even though such a monitor is not required for the diffuser to serve its primary on-orbit calibration function of looking for step-function changes in the instrument response.

3. Solar Calibration Background

The SeaWiFS instrument gains were set to measure the oceans, which are relatively dark compared with the Sun. Accordingly, for solar calibrations of the instrument, the diffuser was designed to have a 10% Lambertian reflectance, with a corresponding bidirectional reflectance distribution function (BRDF) of 0.0318 ($0.10/\pi$).

The SeaWiFS solar diffuser is attached to the side of the instrument and views aft so that it sees the Sun as the satellite passes over the South Pole.[2,3] The diffuser is an aluminum plate with a nominal incidence angle of 60° from normal. The diffuser is coated with YB71 paint, a white thermal control paint with a near-Lambertian BRDF, a high reflectance, and apparent stability in the space environment.[8] As measured by the instrument manufacturer, Santa Barbara Remote Sensing (SBRS), and shown in Fig. 2, the paint is spectrally flat over the wavelength range of SeaWiFS.

An aperture-screen of black anodized aluminum reduces the solar flux on the diffuser. This screen is a plate of 2.54 mm thickness, with holes of 4.32 mm diameter spaced on 6.35 mm centers. The holes were drilled in a pattern rotated 35° from the axes of the screen. The aperture screen has a nominal incidence angle of 30° from normal. The spacing between the screen and the diffuser is such that reflections from the back of the screen onto the diffuser account for less than 1% of the total illumination. The screen configuration and placement provides a uniformly illuminated diffuser surface and reduces the illumina-

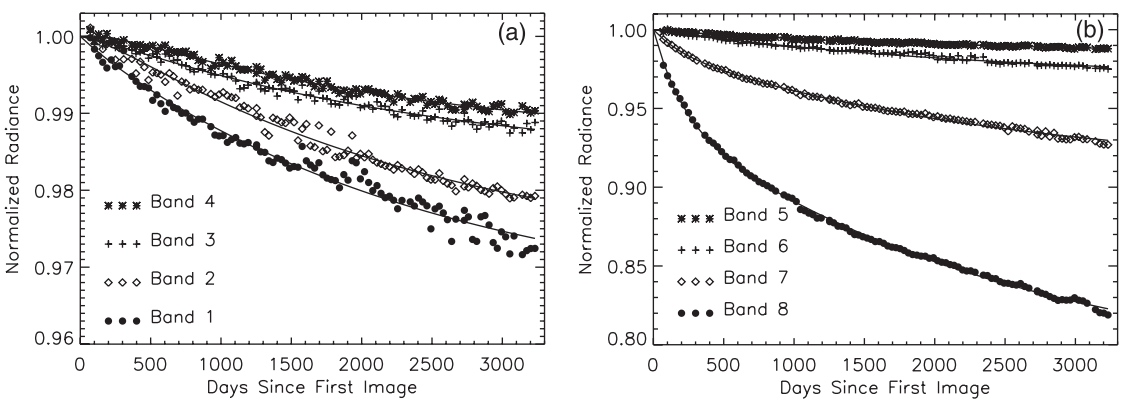

Fig. 1. Lunar calibration time series. The radiometric corrections contained in the calibration table are the inverses of the fits. The vertical scale of the plot for bands 1–4 in (a) is different from the vertical scale of the plot for bands 5–8 in (b).

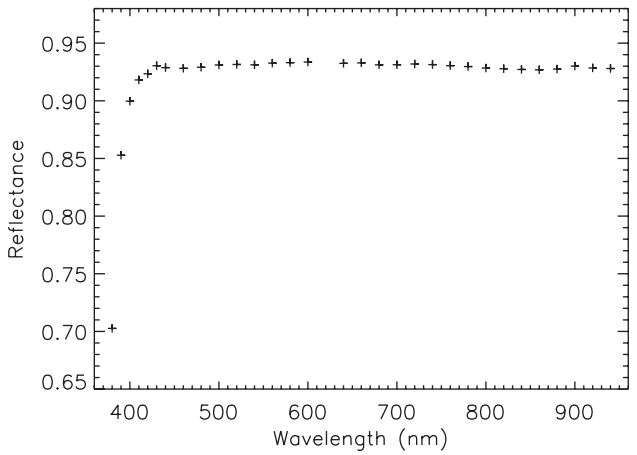

Fig. 2. Reflectance of YB71 paint. The paint is spectrally flat over the wavelength range of SeaWiFS. The measurements are from the SeaWiFS Calibration and Acceptance Data Package, prepared by the instrument manufacturer (Santa Barbara Remote Sensing) for NASA.

tion variations as the incidence angle of the solar irradiance on the diffuser varies over the year.

When SeaWiFS is over the South Pole, the rotation of the satellite (to maintain nadir pointing) causes the Sun to rise and set over the diffuser in the direction of the rotation. Angles around the rotation axis are called elevation in the nomenclature of the SeaWiFS diffuser. Because of the inclination of the satellite's orbit, the incident solar irradiance changes angle on the diffuser over the course of a year in the direction on the diffuser perpendicular to the satellite rotation. This angle is called azimuth in the nomenclature of the SeaWiFS diffuser. Due to the placement of the solar diffuser at the side of the instrument, SeaWiFS observes the diffuser over scan angles of +81° to +99°, while ocean observations occur over scan angles of ±58.29°. Since the solar diffuser is always observed over the same narrow range of scan angles, which lie outside of the scan angle range of the Earth data where the scan modulation had been measured, no scan modulation corrections are applied to the solar calibration data.[4]

The BRDF of the SeaWiFS diffuser was characterized by SBRS prior to launch for bands 4 (510 nm) and 8 (865 nm) at 10 elevation angles (−0.5° to +5.5°) and at 13 azimuth angles (−12.4° to +12.1°) and for all eight bands at normal incidence.[2] The BRDF measurements at normal incidence are shown in Fig. 3. Uncertainties in the BRDF determination are ±3%.[9]

The Cal/Val team has adapted its methodology for processing the on-orbit solar calibration data due to the incomplete determination of the diffuser BRDF. During each solar calibration, the sunlight passes through an elevation angle of 0° on the diffuser, so the mean solar radiances are computed over a 7 × 101 pixel region of the diffuser centered on 0° elevation. The measured BRDF for bands 4 and 8 at this elevation angle are shown in Fig. 3.

The azimuth angles for the SeaWiFS solar calibrations are shown in Fig. 4. The time series shows a two-cycle annual periodicity arising from the variation in the solar incidence angle on the diffuser over the year, along with a secular trend arising from the drift in the node of the satellite's orbit. The satellite orbit has decayed from an initial altitude of 705 km (with a node crossing time of 12:00 noon) to a current altitude of ~690 km (with a node crossing time of ~12:40 p.m.). The node drift is also shown in Fig. 4.

4. Approach to the Solar Data

The Cal/Val team has undertaken an analysis of the mission-long SeaWiFS solar calibration time series spanning some 3100 days from the start of on-orbit operations in September 1997 through early March 2006. The solar calibrations are obtained on the same orbit of each day when the spacecraft is over the South Pole. For each calibration, an average solar radiance, reflected by the solar diffuser, was computed for each band. The operational calibration table was applied to the data to correct for changes in the radiometric response of the instrument over time.[6,7] The resulting time series were normalized to an Earth–Sun distance of one astronomical unit (AU) and the time series for each band was normalized to the first observation in that band. The resulting solar

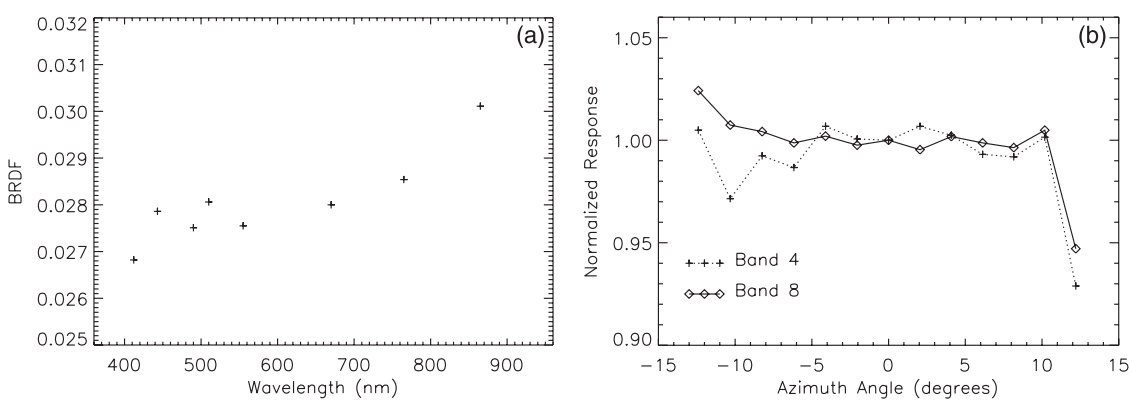

Fig. 3. BRDF of the solar diffuser. (a) BRDF at normal incidence for all eight bands. (b) Response at a 0° elevation angle as a function of azimuth angle, normalized to the response at a 0° azimuth angle.

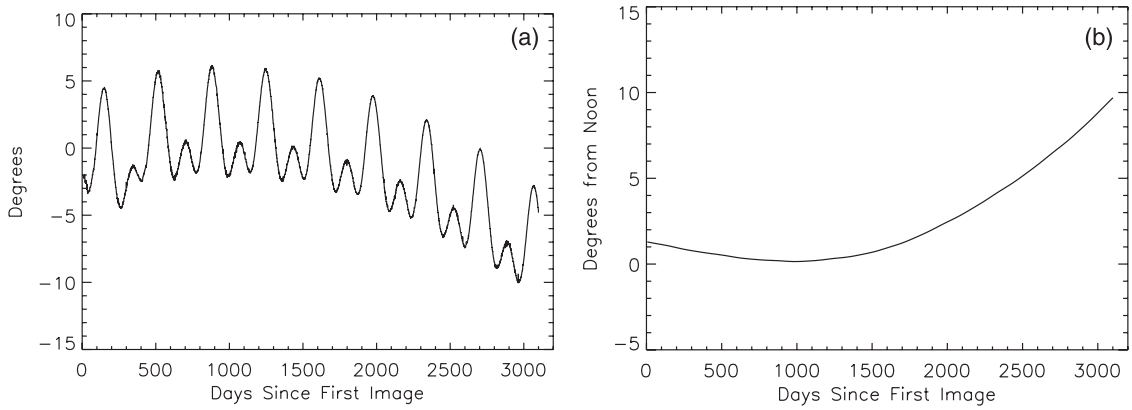

Fig. 4. Azimuthal angles of solar irradiance on the diffuser. (a) Effects of both the solar analema and the orbit node drift are apparent. (b) Drift of the satellite's orbit node crossing. The first SeaWiFS image was obtained at 16:26:30 UT on 4 September 1997.

time series show the normalized diffuser reflectance and the effect of the varying azimuth angles of the solar irradiance over the mission. The time series for band 1 (which shows the largest change in reflectance over the mission) and for band 6 (which shows the smallest change in reflectance over the mission) are shown in Fig. 5.

Comparison of the diffuser time series (Fig. 5) with the azimuth angle time series (Fig. 4) and with the prelaunch diffuser BRDF determinations (Fig. 3) shows why the incomplete characterization of the diffuser BRDF does not allow the Cal/Val team to directly correct the diffuser time series for the effects of the varying azimuth angles. Previous attempts to correct the SeaWiFS solar time series for BRDF effects have concentrated on the first 2 years of the mission.[9,10] Handling the full 9 year time series is complicated because the diffuser BRDF appears to be changing over time. Unlike the Moderate Resolution Imaging Spectrometer[11] (MODIS), SeaWiFS is unable to carry out the type of yaw maneuvers necessary to characterize or monitor changes in the diffuser BRDF on orbit.

To proceed with analyzing the diffuser data, the Cal/Val team has developed a set of empirical corrections for the effects of the azimuth angle variation and the orbit node drift on the diffuser time series. These corrections were derived from multiple linear regressions of the azimuth angle time series and the node drift time series against the diffuser time series. The components of the regressions, chosen to optimize the corrections through a least-squares minimization, are

1. the cosine of the azimuth angles,
2. the sine of the azimuth angles, and
3. the drift in the node of the satellite's orbit.

The regression equation is

$$r(\lambda,\ t) = r_0(\lambda) + r_1(\lambda)\cos[A(t)] + r_2(\lambda)\sin[A(t)] + r_3(\lambda)\Omega(t), \tag{1}$$

where r_i are the regression coefficients, A is the azimuth angle of the solar irradiance on the diffuser, Ω is the node of the satellite's orbit, λ is the SeaWiFS band, and t is the time of the solar observation. The results of the regression for band 1 are shown in Table 2. These results are typical for the other bands. The relative magnitude of the $\cos(A)$ and $\sin(A)$ coefficients show that the annual periodicities in the az-

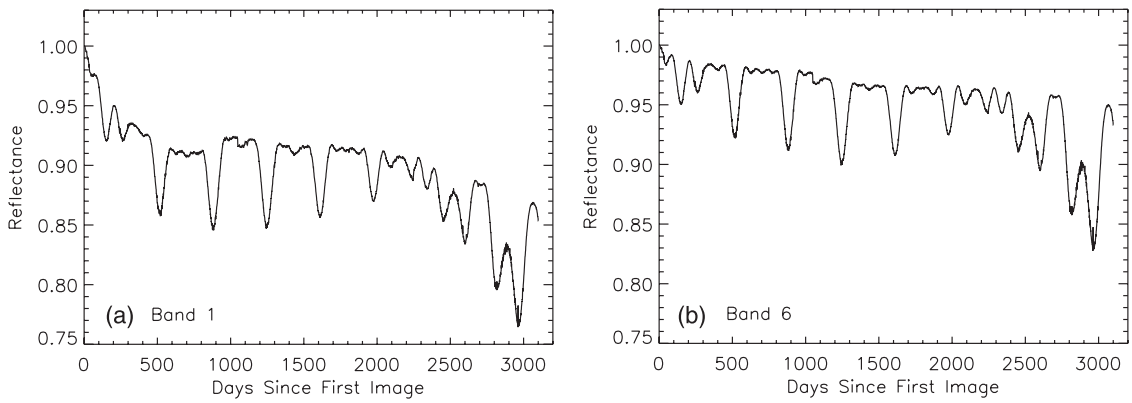

Fig. 5. Solar diffuser time series. Band 1 has the maximum change in diffuser reflectance over time while band 6 has the minimum change in reflectance.

Table 2. Regression Results for Band 1[a]

Coefficient	Magnitude	Uncertainty	Uncertainty (%)
Constant	−8.4	NA	NA
cos(A)	9.4	±0.12	±1.3
sin(A)	−0.21	±0.0059	±2.7
$\mathbf{\Omega}$	−0.0062	±0.00015	±2.5

[a]The dominant uncertainty is for the cos(A) coefficient. The χ^2 for the regression is 0.65.

imuthal angle are not symmetric. Despite the small relative magnitude of the Ω coefficients, inclusion of the orbit node in the regression greatly improves the quality of the fit over the last 2 years of the mission, when the node drifts above 5°. It may be possible to improve the regression fits by subdividing the mission into epochs that are fit individually, but initial attempts to define the epochs have not improved the results over the mission-long fits.

The regression fits yield corrections for each band that normalize the diffuser time series for the varying azimuth angles of the solar irradiance. The corrections for bands 1 and 6 are shown in Fig. 6. These corrections show the effects of both the azimuth angle variations and the orbit node drift. Examination of these two plots shows that corrections of 5%–15% are required for the largest variations in azimuthal angle and that the corrections are largely independent of wavelength. The diffuser BRDF shown in Fig. 3 would yield corrections of only 1%–2% over a similar range of azimuth angles, again showing the necessity of empirical corrections for the azimuth angles.

The diffuser time series, with the corrections applied, are shown in Fig. 7. These time series show the trends in diffuser reflectance over the mission. Comparison of Fig. 7 with Figs. 5 and 6 shows the limitations in this implementation of empirical corrections for the azimuth angle variations. The high-frequency noise in the diffuser time series, which arises from these limitations, does not preclude the analysis of the diffuser reflectance trends.

5. Diffuser Trend Analysis

To begin the diffuser trend analysis, the Cal/Val team examined the diffuser time series for all eight bands to assess possible functional forms to model the trends. While a number of functional forms would fit the data, the team drew on its extensive experience with SeaWiFS lunar data analysis and selected a decaying exponential function of time to model the

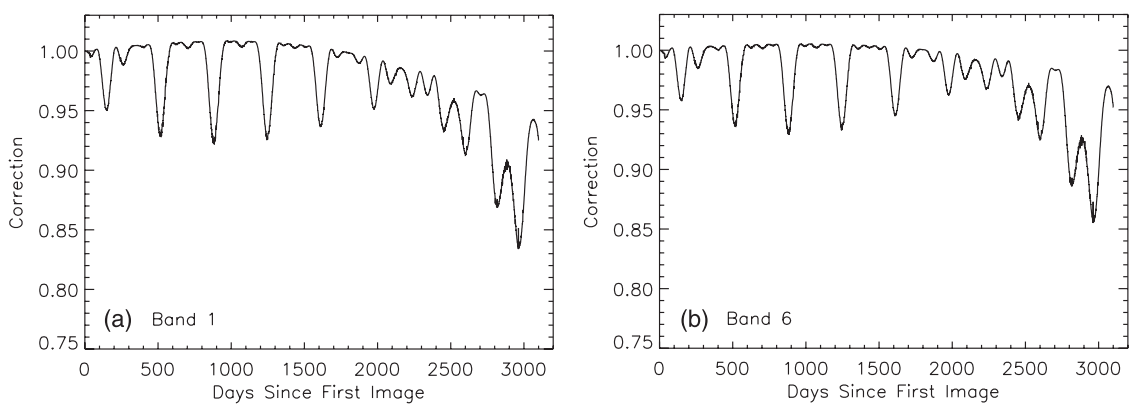

Fig. 6. Azimuthal angle corrections for the diffuser time series. Both corrections show the two-cycle annual periodicities and the secular trend.

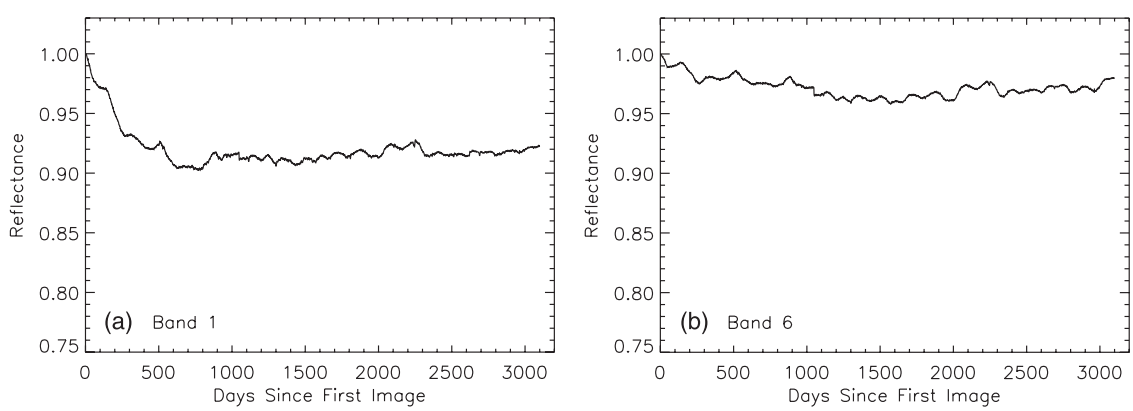

Fig. 7. Diffuser time series corrected for azimuthal angles. The time series show the trends in diffuser reflectance. The high-frequency noise is due to limitations in empirical corrections for the azimuthal angle variations.

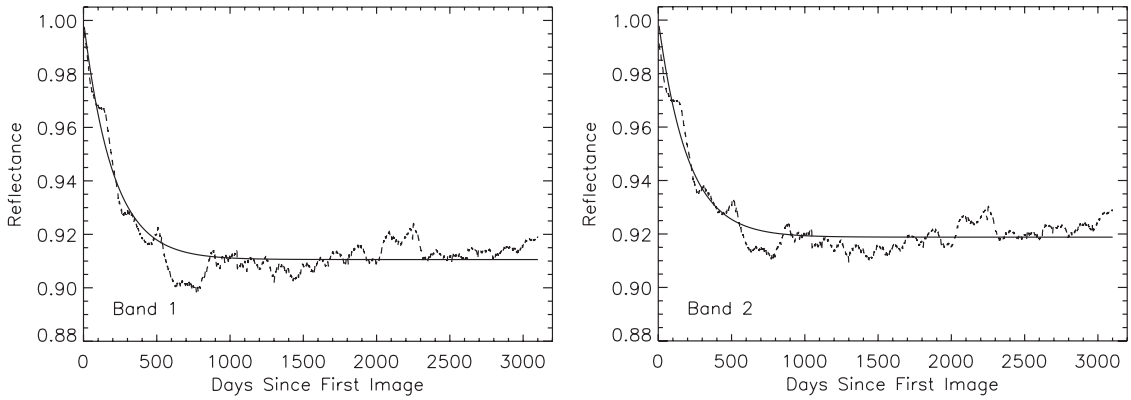

Fig. 8. Diffuser time series for bands 1 and 2. The solar diffuser time series are fit by decaying exponential functions with 200 day time constants. The exponentials fit the reflectance trends through the noise from the azimuthal angle corrections.

diffuser trends. Decaying exponentials are consistent with possible mechanisms of diffuser reflectance degradation: coating of optical surfaces by photolyzed organic materials outgassed from the spacecraft or reflectance degradation under exposure to UV radiation.

For the trend analysis, the Cal/Val team fit the solar diffuser time series with a decaying exponential function of time for each band. These functions have the form

$$f(\lambda,\ t) = a_0(\lambda) - a_1(\lambda)\{1 - \exp[-a_2(\lambda)(t - t_0)]\}, \quad (2)$$

where a_0 is the initial value of the function, a_1 is the amplitude of the exponential function, a_2 is the time constant of the exponential function, λ is the SeaWiFS band, t is the time of the observation, and t_0 is the reference time for the time series. In the initial analysis of the time series, the time constant of the exponential was a free parameter in the fits. Bands 1–3, which exhibit the greatest change in reflectance over time, and thus provide the most accurate determination of the exponential time constants, yielded time constants of 173, 203, and 250 days, respectively. Such short-period time constants are consistent with diffuser degradation from the outgassing of materials from the spacecraft. At the same time, a 200 day period is the optimum time constant determined for the short-period exponential in the lunar calibration time series.[7] Since outgassing would give rise to the same time constants for all eight bands, and drawing on the experience with the lunar data, the Cal/Val team decided to apply a single 200 day time constant to the diffuser analysis for all eight bands.

The diffuser time series for all eight bands are shown in Figs. 8–11. The fits in the plots show the trends in the diffuser reflectance with time. Comparing these plots shows the wavelength dependence of the change in diffuser reflectance over the mission. For all eight bands, the change in reflectance has essentially flattened out after 1000 days, showing that the exponential time constant of 200 days, which fits the behavior of bands 1–4 quite well, also works for bands 5–8. The residuals from the fits, shown in Fig. 12, are within 2% for each band. These residuals show the combined uncertainties in the azimuth angle corrections and in the diffuser trend fits. There are low-frequency and high-frequency periodic signals apparent in all of the bands, including band-specific features that arise from the azimuth angle corrections. Both sets of periodic signals likely arise from the incomplete correction to the diffuser time series provided by the regression fits. An incomplete correction for the diffuser BRDF would give rise

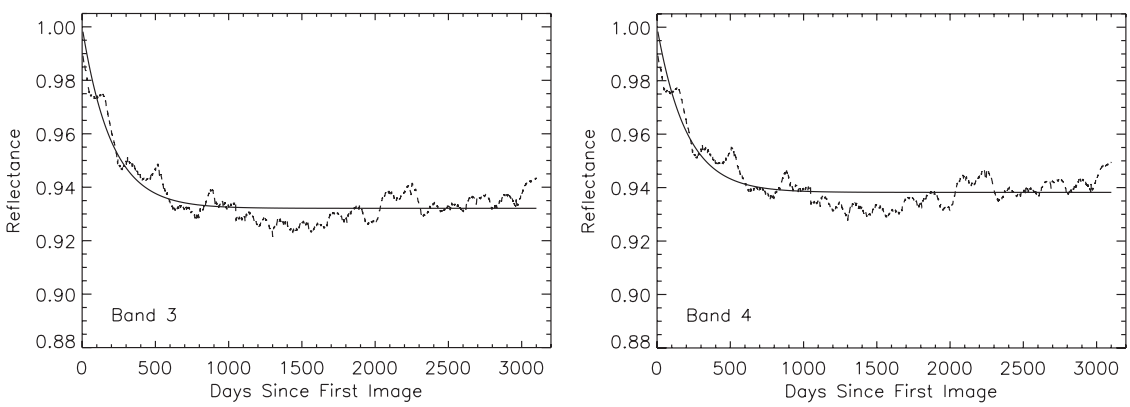

Fig. 9. Diffuser time series for bands 3 and 4.

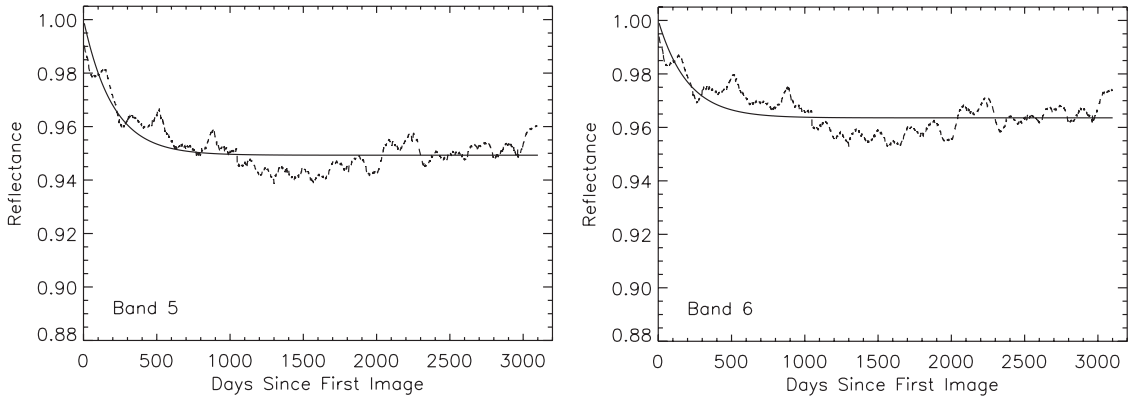

Fig. 10. Diffuser time series for bands 5 and 6.

to a high-frequency signal, while an incomplete correction for the orbit node drift would give rise to a low-frequency signal.

The solar diffuser housing design does not fully block out earthshine on the diffuser under all possible observing conditions. Consequently, as the orbit node drifts away from local noon, the possibility of earthshine reflected from clouds and ice impinging on the diffuser during solar calibrations increases. Since solar calibrations are not used to monitor the radiometric stability of SeaWiFS, the Cal/Val team has not undertaken studies to quantify the level of earthshine on the SeaWiFS diffuser, as has been recently done for MODIS.[12,13]

The decrease in diffuser reflectance over the mission is wavelength dependent, ranging from 9% in the blue (412 nm) to 5% in the red and near infrared (670–865 nm). This trend is apparent in Fig. 13, where the fits to the trends in diffuser reflectance for all eight bands are shown. The degradation of diffuser reflectance is similar to the degradation in the SeaWiFS radiometric response observed for bands

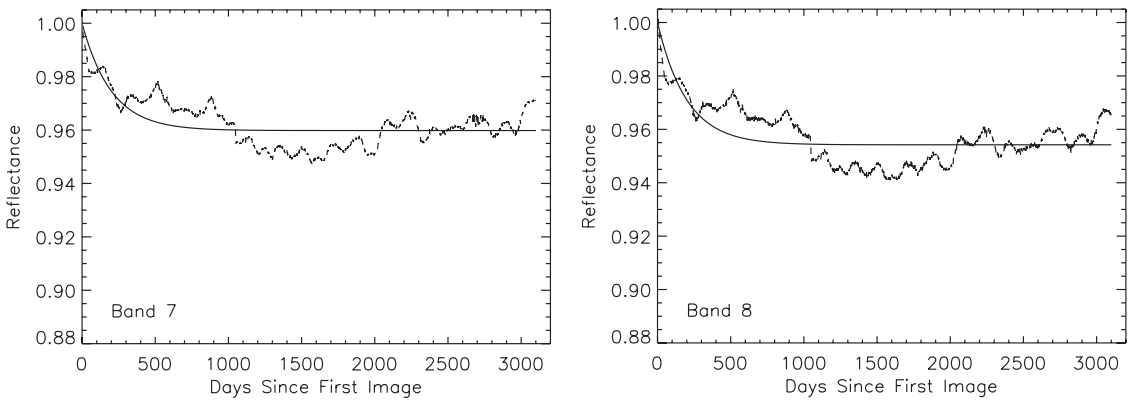

Fig. 11. Diffuser time series for bands 7 and 8.

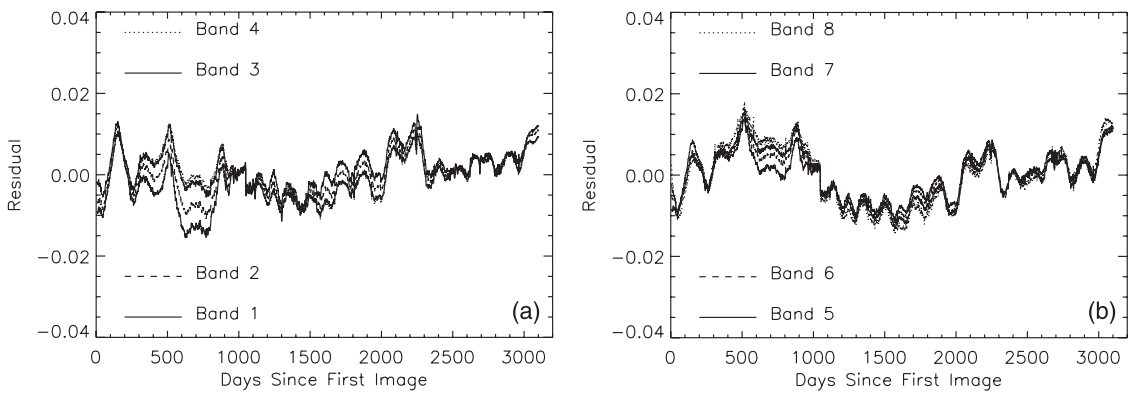

Fig. 12. Residuals of diffuser reflectance fits. The residuals are within 2% for each band. The residuals show both low-frequency and high-frequency signals, though the low-frequency signals are more pronounced for bands 5–8.

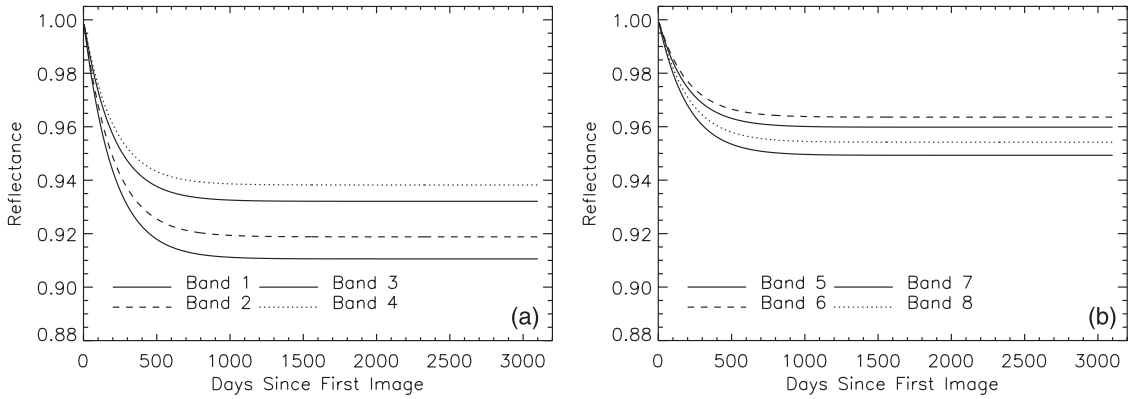

Fig. 13. Fits to diffuser reflectances. The exponential fits to the diffuser reflectance time series have time constants of 200 days.

1–5 (412–555 nm) from the lunar calibration time series,[5,6] though the magnitude of the change is four times larger for the diffuser. Since the diffuser data have been corrected for the radiometric response of the instrument, the change in diffuser reflectance provides an independent example of the degradation mechanism that affects both the solar diffuser and telescope optics in the blue and green bands. Possible mechanisms include the coating of the optical surfaces by photolyzed organic materials outgassed from the spacecraft and reflectance degradation under UV exposure, as was reported for the YB71-coated Full Aperture Solar Calibrator (FASC) on the Landsat-7 Enhanced Thematic Mapper+ (ETM+).[14] For either process, the telescope optics are more protected than the diffuser, so the diffuser degradation is greater than the optics degradation for bands 1–5 (412–555 nm). The flattening of the diffuser degradation after 1000 days is more consistent with outgassing as the degradation mechanism than with UV exposure.

6. Signal-to-Noise Ratio Analysis

The initial requirements for SeaWiFS established by NASA included a minimum signal-to-noise ratio (SNR) for each band measured at ocean typical radiances (L_{typ}).[1] The prelaunch characterization of the instrument by SBRS showed that the measured SNR exceeded the specifications by a wide margin for each band.[15] As part of the prelaunch characterization, the Cal/Val team developed a sensor noise model for SeaWiFS.[15] The linear model, based on the noise levels of the instrument, predicts SNRs for given input radiances. Table 3 provides the specifications, noise model results, and prelaunch measurements of the SNRs for SeaWiFS. The noise model yields slightly higher computed SNRs than were measured at L_{typ}.

Monitoring the SNR of an instrument on orbit is one method of ensuring that the instrument and the data it produces continue to meet the performance specifications. The determination of the SNR on orbit is problematic in that the measurement requires a uniformly illuminated light source that fills the instrument aperture and is constant over time. A complicating factor in comparing on-orbit results with prelaunch values is that uniform illumination levels on orbit are generally at radiance levels other than L_{typ}. Nonetheless, building on the diffuser trend analysis discussed above, the Cal/Val team has developed a methodology for computing the on-orbit SNRs for SeaWiFS from the solar diffuser data.

The calibration of the solar observations corrected the data for changes in the radiometric response of the instrument over time, for the temperature dependences of the detector responses, and for the varying Earth–Sun distance. The diffuser trend analysis discussed above provides corrections to the diffuser time series for the varying azimuth angles of the solar irradiance and for the degradation of the diffuser reflectance over time, where the reflectance degradation corrections are the inverses of the exponential fits shown in Fig. 13. The fully corrected diffuser time series is

$$L'(\lambda, t) = L(\lambda, t)/r(\lambda, t)/f(\lambda, t), \tag{3}$$

where L is the calibrated solar radiance reflected by the diffuser, normalized to 1 AU; r is the correction for varying azimuthal angles; f is the correction for the degradation of the diffuser reflectance; λ is the SeaWiFS band; and t is the time of the observation. The corrected diffuser time series provides a uniformly illuminated, stable, full-aperture light source

Table 3. SeaWiFS Prelaunch SNRs[a]

Band	λ	L_{typ}	SNR Specifications	Model SNR	Measured SNR
1	412	9.10	499	990	940
2	443	8.41	674	1091	950
3	490	6.56	667	1170	1156
4	510	5.64	616	1152	1055
5	555	4.57	581	1069	963
6	670	2.46	447	781	798
7	765	1.61	455	859	860
8	865	1.09	467	726	670

[a]The SNRs are measured at L_{typ}, the units of which are mW cm^{-2} μm^{-1} sr^{-1}.

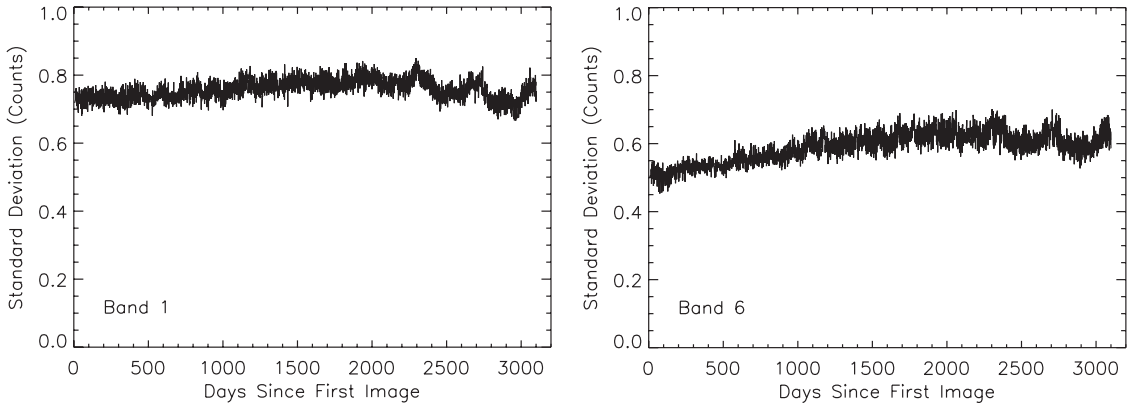

Fig. 14. Noise estimate time series for bands 1 and 6. The noise estimates are the standard deviations of the mean solar radiances for the individual diffuser observations.

for SeaWiFS. The on-orbit SNRs can be calculated from

$$\mathrm{SNR}(\lambda, t) = \frac{\langle L'(\lambda, t)\rangle}{\sigma[\langle L'(\lambda, t)\rangle]}, \tag{4}$$

where the standard deviations of the mean radiances for the individual diffuser observations serve as the noise estimates. These noise estimates are stable over the mission with values of less than one count for each band. Time series of the noise estimates for bands 1 and 6, which are typical of the other bands, are shown in Fig. 14, while the means of the noise estimates over the mission are shown for each band in Table 4.

Table 4. SeaWiFS On-Orbit Mean Noise Estimates[a]

Band	Wavelength	Noise Estimate
1	412	0.757 ± 0.030
2	443	0.658 ± 0.040
3	490	0.481 ± 0.036
4	510	0.659 ± 0.055
5	555	0.464 ± 0.042
6	670	0.590 ± 0.044
7	765	0.389 ± 0.076
8	865	0.562 ± 0.036

[a]The noise estimates are the standard deviations of the mean solar radiances for the individual diffuser observations, in counts.

The SNR time series for all eight bands are shown in Figs. 15–18. The differences in the time series for individual bands arise from variations in the solar data. The two primary sources of uncertainty in these SNR computations are the diffuser degradation trend residuals (Fig. 12) and the uncertainties in the standard deviations of the mean irradiances used in the noise estimates (Fig. 14). The scatter in the SNR data shown in these plots and in the noise time series (Fig. 14) most likely arise from small variations in the illumination of the aperture screen and of the solar diffuser from one solar calibration to the next. To estimate the change in SNR over the mission, despite the scatter in the data, the Cal/Val team performed a linear fit to the time series for each band. Since the solar radiances reflected by the diffuser are at illumination levels other than L_{typ}, the Cal/Val team used the sensor noise model to compute SNRs for the mean radiances reflected by the diffuser for the first 30 solar calibrations of the mission:

$$L_{diff}(\lambda) = \langle L'(\lambda,\ t_0 : t_1)\rangle, \tag{5}$$

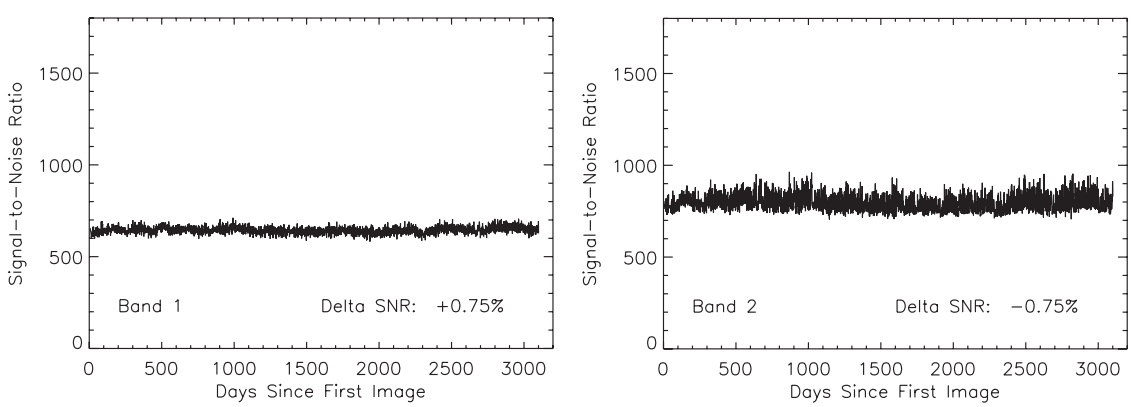

Fig. 15. SNRs for bands 1 and 2. The SNR time series are fit by linear functions of time to estimate the change in SNR over the mission. That change is shown in each plot.

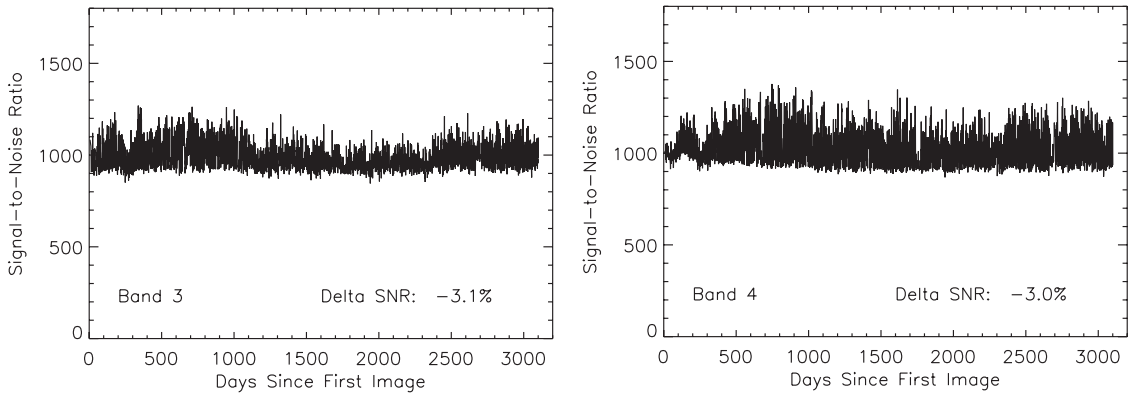

Fig. 16. SNRs for bands 3 and 4.

where λ is the SeaWiFS band, t_0 is the time of the first observation, and t_1 is the time of the 30th observation. Table 5 shows the radiance levels, model SNR, and the derived SNR from this analysis for each band. The initial (September 1997) and current (March 2006) SNR values are the end points of the linear fits to the SNR time series. As discussed above, the uncertainties in the computed on-orbit SNR [σ(SNR)] are the combined uncertainties from the degradation trends (shown in Fig. 12) and from the noise time series (shown in Table 4 and Fig. 14). The changes in the on-orbit SNR [Δ(SNR)] are the differences in the initial and current values. Examination of the results presented in Table 5 shows that the agreement between the noise model SNRs and the derived on-orbit SNRs is comparable to that between the noise model SNRs and the prelaunch SNRs shown in Table 3. The changes in SNRs over the mission are less than 7% and lie within the uncertainties of the SNR measurements. The uncertainties in the SNRs do not show strong correlations with either the trends in the radiometric response of the instrument (Fig. 1) or the diffuser degradation trends (Fig. 13). The conclusion that can be drawn from this

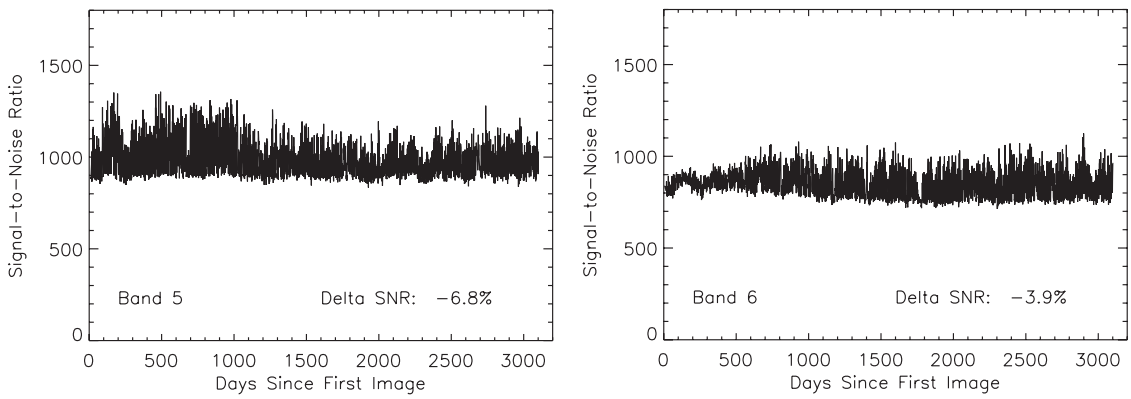

Fig. 17. SNRs for bands 5 and 6.

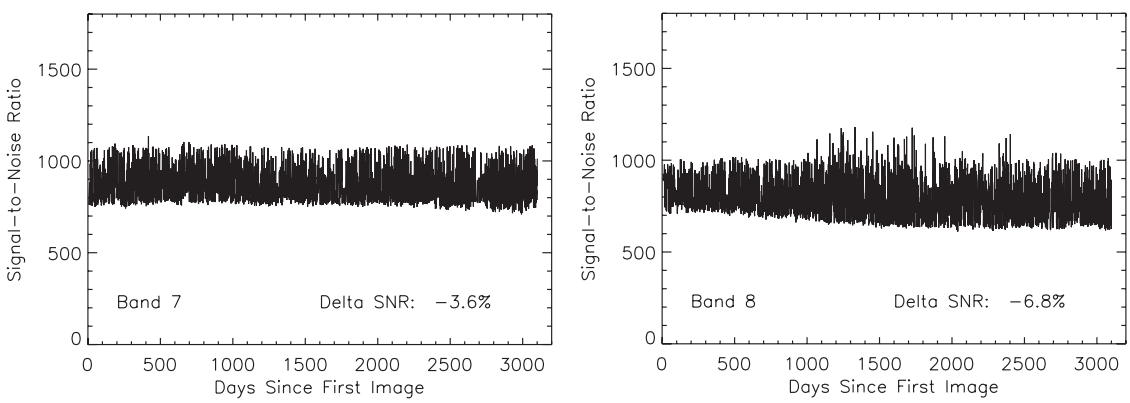

Fig. 18. SNRs for bands 7 and 8.

Table 5. SeaWiFS On-Orbit SNRs[a]

Band	λ	L_{diff}	Model SNR	Initial SNR	Current SNR	σ(SNR) (%)	Δ(SNR) (%)
1	412	4.44	736	642	646	±3.4	+1
2	443	5.19	784	800	794	±5.7	−1
3	490	5.45	955	1007	976	±7.5	−3
4	510	5.33	943	1044	1013	±9.5	−3
5	555	5.18	859	1023	953	±9.6	−7
6	670	4.43	572	867	833	±8.5	−4
7	765	3.63	668	888	857	±11	−4
8	865	2.99	557	824	767	±14	−7

[a]The SNRs are measured at L_{diff}, the units of which are mW cm^{-2} μm^{-1} sr^{-1}. σ(SNR) is the uncertainty in the computed SNR. Δ(SNR) is the change from the initial SNR to the current SNR.

analysis of the on-orbit SNRs is that SeaWiFS continues to exceed the prelaunch specifications for SNRs after more than 3100 days into the mission.

7. Discussion

Since SeaWiFS has completed the ninth year of its mission, analysis of the solar calibration data provides a unique opportunity to study long-term trends in solar diffuser reflectance on orbit. Because the primary monitor of the radiometric stability of SeaWiFS is the Moon, the diffuser trends are decoupled from trends in the instrument response.

The residual effects of the azimuth angle variations in the SeaWiFS diffuser time series (Figs. 8–11) show the necessity of accurately determining the BRDF of diffusers prior to launch and the necessity of monitoring the changes in both the BRDF of and the reflectance of diffusers on orbit. The long-term degradation of the reflectance of solar diffusers on orbit, and the monitoring and modeling of that degradation, is a critical concern for Earth remote sensing instruments that employ solar diffusers as the primary on-orbit radiometric calibration standard for reflective solar (visible, near-infrared, and shortwave infrared) bands.

The reflectance degradation trends for the SeaWiFS solar diffuser (Fig. 13) show that diffusers made from YB71-coated aluminum exhibit decreases in reflectance over time that can be fit by decaying exponentials with relatively short time constants (200 days for SeaWiFS). The degradation is wavelength dependent, with the blue bands degrading 9% while the red bands degrade 5%. For all of the bands, the degradation levels off after the first thousand days on orbit. The most likely degradation mechanism is coating of optical surfaces by photolyzed organic materials outgassed from the spacecraft. These results imply that for other instruments that use diffusers as the primary monitor of radiometric response, trends in the diffuser response that continue significantly beyond 1000 days probably arise from either continued outgassing events from the spacecraft or ongoing changes in the instrument response.

The Landsat-7 ETM+ is one remote sensing instrument, other than SeaWiFS, that uses a YB71-coated solar diffuser (the FASC). The SeaWiFS diffuser results are difficult to compare with those reported for the ETM+ FASC, since estimates of the FASC reflectance on orbit are provided for only a limited number of observations.[14]

The SeaWiFS diffuser results are qualitatively similar to those observed for the EOS Terra MODIS solar diffuser,[11] which is made from space-grade Spectralon. The complicated on-orbit history of the Terra MODIS instrument and the poor characterization of the SeaWiFS diffuser BRDF makes detailed comparisons of the SeaWiFS and MODIS diffusers difficult. However, comparisons of the long-term degradation trends of the SeaWiFS diffuser to both the EOS Terra and Aqua MODIS diffusers should provide insight into the on-orbit performance of solar diffusers on future Earth remote sensing instruments, such as the Visible and Infrared Radiometer Suite, scheduled to fly on the NPP and NPOESS satellites and the Advanced Baseline Imager, scheduled to fly on the GOES-R series satellites.

The solar calibration data analysis presented here provides a methodology for computing the SNRs for SeaWiFS on orbit from solar data that has been corrected for both the varying solar incidence angles on the diffuser and for the degradation in diffuser reflectance. Comparison of the on-orbit SNRs with noise model SNRs, prelaunch SNRs, and the instrument specifications shows that changes in the SNRs over the mission are less than 7% and are within the measurement uncertainties (Table 5). The SNR for each SeaWiFS band still exceeds the prelaunch specification. Similar diffuser data analysis methodologies can be developed to monitor the on-orbit SNRs other remote sensing instruments.

References

1. C. R. McClain, W. E. Esaias, W. Barnes, B. Guenther, D. Endres, S. B. Hooker, B. G. Mitchell, and R. Barnes, *SeaWiFS Calibration and Validation Plan,* NASA Tech. Memo 104566, S. B. Hooker and E. R. Firestone, eds. (NASA Goddard Space Flight Center, 1992), Vol. 3.
2. R. A. Barnes and R. E. Eplee, "The SeaWiFS solar diffuser," in *SeaWiFS Calibration Topics, Part 1,* NASA Tech. Memo 104566, S. B. Hooker and E. R. Firestone, eds. (NASA Goddard Space Flight Center, 1996), Vol. 39, pp. 54–61.
3. R. A. Barnes, R. E. Eplee, Jr., F. S. Patt, and C. R. McClain, "Changes in the radiometric stability of SeaWiFS determined from lunar and solar-based measurements," Appl. Opt. **38,** 4649–4664 (1999).
4. R. A. Barnes, A. W. Holmes, W. L. Barnes, W. E. Esaias, C. R. McClain, and T. Svitek, *SeaWiFS Prelaunch Radiometric Calibration and Spectral Characterization,* NASA Tech. Memo 104566, S. B. Hooker, E. R. Firestone, and J. G. Acker, eds. (NASA Goddard Space Flight Center, 1994), Vol. 23.
5. R. A. Barnes, R. E. Eplee, Jr., G. M. Schmidt, F. S. Patt, and C. R. McClain, "Calibration of SeaWiFS. I. Direct techniques," Appl. Opt. **40,** 6682–6700 (2001).
6. R. E. Eplee, Jr., R. A. Barnes, F. S. Patt, G. Meister, and C. R. McClain, "SeaWiFS lunar calibration methodology after six years on orbit," in *Earth Observing Systems IX,* W. L. Barnes and J. J. Butler, eds., Proc. SPIE **5542,** 1–13 (2004).
7. R. E. Eplee, Jr., S. W. Bailey, R. A. Barnes, H. H. Kieffer, and C. R. McClain, "Comparison of SeaWiFS on-orbit lunar and

vicarious calibrations," in *Earth Observing Systems XI,* J. J. Butler and X. Xiong, eds., Proc. SPIE **6296,** 629639 (2006).
8. A. C. Tribble, R. Lukis, E. Watts, V. A. Borisov, S. A. Demidov, V. A. Denisenko, A. A. Gorodetskiy, V. K. Grishin, S. F. Nauma, V. K. Sergeev, and S. P. Sokolova, "United States and Russian thermal control coating results in low earth orbit," J. Spacecraft Rockets **33,** 160–166 (1996).
9. R. A. Barnes and E. F. Zalewski, "Reflectance-based calibration of SeaWiFS. I. Calibration coefficients," Appl. Opt. **42,** 1629–1647 (2003).
10. R. A. Barnes and E. F. Zalewski, "Reflectance-based calibration of SeaWiFS. II. Conversion to radiance," Appl. Opt. **42,** 1648–1650 (2003).
11. X. Xiong, H. Erives, S. Xiong, X. Xie, J. Esposito, J. Sun, and W. Barnes, "Performance of terra MODIS solar diffuser and solar diffuser stability monitor," in *Earth Observing Systems X,* J. J. Butler, ed., Proc. SPIE **5882,** 58820S (2005).
12. R. E. Wolfe, W. Esaias, A. I. Lyapustin, and X. Xiong, "MODIS solar diffuser earthshine modeling and analysis," in *Earth Observing Systems XI,* J. J. Butler and X. Xiong, eds., Proc. SPIE **6296,** 629607 (2006).
13. X. Xie, X. Xiong, R. E. Wolfe, and A. I. Lyapustin, "Improvement of MODIS RSB calibration by minimizing the earthshine impact on solar diffuser observations," in *Earth Observing Systems XI,* J. J. Butler and X. Xiong, eds., Proc. SPIE **6296,** 629609 (2006).
14. B. L. Markham, J. L. Barker, E. Kaita, J. Sieferth, and R. Morfitt, "On-orbit performance of the Landsat-7 ETM+ radiometric calibrators," Int. J. Remote Sens. **24,** 265–286 (2003).
15. R. A. Barnes, W. L. Barnes, W. E. Esaias, and C. R. McClain, *Prelaunch Acceptance Report for the SeaWiFS Radiometer,* NASA Tech. Memo 104566, S. B. Hooker, E. R. Firestone, and J. G. Acker, eds. (NASA Goddard Space Flight Center, 1994), Vol. 22.